Partition Coefficient of a Surfactant Between Aggregates and Solution: Application to the Micelle-Vesicle Transition of Egg Phosphatidylcholine and Octyl β-D-Glucopyranoside

Maïté Paternostre, Olivier Meyer, Cécile Grabielle-Madelmont, Sylviane Lesieur, Magdy Ghanam, and Michel Ollivon

Equipe "Physicochimie des Systèmes Polyphasés," Université Paris Sud, 92296 Châtenay-Malabry Cedex, France

ABSTRACT The mechanism of the solubilization of egg phosphatidylcholine containing 10% (M/M) of egg phosphatidic acid unilamellar vesicles by the nonionic detergent, octyl β-D-glucopyranoside, has been investigated at both molecular and supramolecular levels by using fluorescence and turbidity measurements. In the lamellar region of the transition, the solubilization process has been shown to be first a function of the initial size before reaching an equilibrium aggregation state at the end of this region (the onset of the micellization process). The analysis during the solubilization process of the evolution of both the fluorescence energy transfer between N-(7-nitro-2,1,3-benzoxadiazol-4-yl)-phosphatidylethanolamine (NBD-PE) and N-(lissamine rhodamine B sulfonyl)-phosphatidylethanolamine (Rho-PE) and the fluorescence of 6-dodecanoyl-2-dimethylaminonaphtalene (Laurdan) has allowed us to determine the evolution of the detergent partitioning between the aqueous and the lipidic phases, i.e., the evolution of the molar fraction of OG in the aggregates ($X_{OG/Lip}$) with its monomeric detergent concentration in equilibrium ($[OG]_{H_2O}$), throughout the vesicle-to-micelle transition without isolating the aqueous medium from the aggregates. The curve described by $X_{OG/Lip}$ versus $[OG]_{H_2O}$ shows that the partition coefficient of OG is changing throughout the solubilization process. From this curve, which tends to a value of 1/(critical micellar concentration), five different domains have been delimited: two in the lamellar part of the transition (for $0 < [OG]_{H_2O} < 15.6$ mM), one in the micellization part, and finally two in the pure micellar region (for $16.5 < [OG]_{H_2O} < 21$ mM). The first domain in the lamellar part of the transition is characterized by a continuous variation of the partition coefficient. In the second domain, a linear relation relates $X_{OG/Lip}$ and $[OG]_{H_2O}$, indicating the existence of a biphasic domain for which the detergent presents a constant partition coefficient of 18.2 M^{-1}. From the onset to the end of the solubilization process (domain 3), the evolution of ($X_{OG/Lip}$) with $[OG]_{H_2O}$ can be fitted by a model corresponding to the coexistence of detergent-saturated lamellar phase with lipid-saturated mixed micelles, both in equilibrium with an aqueous phase, i.e., a three-phase domain. The micellar region is characterized first by a small two-phase domain (domain 4) with a constant partition coefficient of 21 M^{-1}, followed by a one-phase mixed-micellar domain for which $X_{OG/Lip}$ no longer linearly depends on $[OG]_{H_2O}$. The results are discussed in terms of a phase diagram.

INTRODUCTION

In membrane biology and biophysics, it is of importance to monitor the formation of artificial membranes to be able to study precisely the activity of a membrane protein, to determine some of its particular structural aspects, and/or to modify intrinsic parameters of the membrane (lipid composition, protein density, etc.). Moreover, the potential applications of liposomes are becoming more and more important (drug delivery and targeting, cosmetology, and farm industry). For these reasons, it is essential to build new approaches for the characterization of liposomes but also to identify and characterize the structural intermediates leading to the formation of these liposomes. Indeed, these studies should lead to the control of the final size and structure of the liposomes, of the physical chemistry of the membrane

(permeability, fluidity, etc.), and of course to monitoring of the protein incorporation process.

This work deals with the lamellar-to-micellar transition induced by surfactant molecules (detergents). Although numerous studies have been made of this transition (Ollivon et al., 1988; Paternostre et al., 1988; Rigaud et al., 1988; Schubert and Schmidt, 1988; Lichtenberg and Barenholz, 1988; Ueno, 1989; Edwards et al., 1989; da Graça Miguel et al., 1989; Vinson et al., 1989; Urbaneja et al., 1990; Lasch et al., 1990; Walter, 1990; Walter et al., 1991; Inoue et al., 1992), the molecular and the supramolecular mechanisms of the transition are still not yet fully elucidated from a physicochemical point of view. Indeed, even if the transition has been defined at each boundary of the solubilization and/or the reconstitution stages by the molecular composition of the mixed detergent-lipid aggregates and by the detergent concentration in the aqueous continuum, the intermediate structures and the evolution of their compositions throughout the vesicle-to-micelle transition are not yet completely understood. Information about the supramolecular level of the transition has already been obtained by light-scattering measurements, i.e., the determination of the phase boundaries of the vesicle-to-micelle transition

(Ollivon et al., 1988; Paternostre et al., 1988; Urbaneja et al., 1990; Inoue et al., 1992; Seras et al., 1992, 1993) and of the solubilization of native biomembranes (del Rio et al., 1991; Meyer et al., 1992; Kragh-Hansen et al., 1993). The structure, the shape, and the size evolution of the mixed aggregates appearing during the transition have been determined by cryotransmission electron microscopy (Edwards et al., 1989; Vinson et al., 1989; Walter et al., 1991).

On the molecular level, Ollivon et al. (1988) and Eidelman et al. (1988) have used resonance fluorescence energy transfer between two membrane probes to characterize the aggregation states at specific steps of the transition. However, these experiments did not allow the determination of the partition coefficient of the detergent throughout the solubilization process. This has been done by equilibrium dialysis and by using radiolabeled detergent (Ueno, 1989; Kragh-Hansen et al., 1993), by gel filtration chromatography and rapid-filtration on glass fiber filters (le Maire et al., 1987), by hygroscopic desorption (Conrad and Singer, 1981), and by combination of density gradient, equilibrium dialysis, and gel exclusion chromatography (Schubert and Schmidt, 1988). All of these techniques have the nontrivial disadvantage of having to separate the mixed aggregates from the aqueous medium, which often requires long and tedious experiments and sometimes results in material loss. The evolution of an appropriate property, i.e., permeability measurements (Rigaud et al., 1988) the absorption or the fluorescence of a soluble amphiphile (De Foresta et al., 1990), or the absorption (Meyer et al., 1992) or the activity (De Foresta et al., 1990) of a membrane protein, was also exploited to determine, during the incorporation of an amphiphile in a lipidic membrane, the partition between the solution and the membrane.

In this work we have analyzed the evolution of the fluorescent properties of membrane probes during the solubilization process of egg phosphatidylcholine/egg phosphatidic acid (90/10 molar ratio) induced by the non-ionic surfactant octyl-β-D-glucopyranoside (OG). The partition coefficients of OG between the solution and the aggregates were determined throughout the solubilization process by using membrane fluorescent probes: 6-dodecanoyl-2-dimethylaminonaphthalene (Laurdan) on one hand and the couple (N-(7-nitro-2,1,3-benzoxadiazol-4-yl)-phosphatidylethanolamine)/(N-(lissamine rhodamine B sulfonyl)phosphatidylethanolamine) (NBD-PE/Rho-PE) on the other. In addition, the influence of the initial vesicle sizes on the solubilization pathway has been examined by simultaneous turbidity and Laurdan fluorescence measurements.

MATERIALS AND METHODS

Chemicals

Egg phosphatidylcholine (EPC) and egg phosphatidic acid (EPA) were purchased from Avanti and Sigma, respectively, and used without any further purification. 6-Dodecanoyl-2-dimethylaminonaphthalene (Laurdan), N-(7-nitro-2,1,3-benzoxadiazol-4-yl)phosphatidylethanolamine (NBD-PE), and N-(lissamine rhodamine B sulfonyl)phosphatidylethanol-

amine (Rho-PE) were purchased from Molecular Probes, and octyl-β-D-glucopyranoside (OG) was from Sigma. All of the experiments were performed in a buffered solution of the following composition: HEPES, 10 mM and NaCl, 145 mM, pH = 7.4.

Liposome preparation

Liposomes were prepared by the reverse-phase evaporation technique (REV) described by Szoka and Papahadjopoulos (1978) and sequentially extruded through Nucleopore filters of 0.8, 0.4, 0.2, 0.1, and 0.05 μm diameter to form large unilamellar vesicles that were uniform in size and about 150 nm in diameter. For the formation of REVs a mixture of EPC and EPA (90/10% molar ratio) was used. Laurdan was inserted in the lipid chloroformic solution at a probe/lipid molar ratio of 0.15%, whereas NBD-PE and Rho-PE were inserted in the lipid chloroformic solution at a probe-to-lipid molar ratio of 1% each.

Liposome sizing

High-performance gel exclusion chromatography

Gel exclusion HPLC analysis was performed using the experimental conditions given by Ollivon et al. (1986) and Lesieur et al. (1991). A 30 × 0.75 cm TSK G6000 PW column supplied by TOYO SODA (Tokyo, Japan), was obtained from Beckman (Berkeley, CA). The column was preceded by a 2-μm filter (Rheodyne, CA). The HPLC apparatus was equipped with a Hitachi pump (model L-6000) and an injection valve (Rheodyne). The eluant was the aqueous buffer used for vesicle preparation. Before each analysis series, the column was saturated with phospholipid vesicles. Vesicle dispersion loading was 200 μl. Sample detection was performed by optical density measurements with a Hitachi multichannel detector (model L-3000) in a 200- to 360-nm range. The data were directly transferred to a computer and analyzed by means of appropriate software (Lesieur et al., 1993).

The column parameter K_d was calculated from the relation

$$K_d = (V_e - V_o)/(V_t - V_o) \qquad (1)$$

V_e, V_t, and V_o are the sample elution, and the total and the effective exclusion volumes respectively. The total volume ($V_t = 11.43$ ml) of the column was determined from the elution of sodium azide. The void volume ($V_o = 4.40$ ml) was taken at the intercept of the baseline, with the half-height tangent to the left side of the peak corresponding to the elution of excluded large vesicles (in our case the largest vesicles contained in unextruded REVs). Elution volumes of the sample corresponding to the maximum of the chromatograms (V_e) were determined by the intercept of the half-height tangent of the HPLC symmetrical peaks.

The sample K_d was then related to the size of the vesicles by using the following relation established for the column by Lesieur et al. (1991):

$$\log(MD) = 3.03 - 4.43\,(K_d) + 9.63\,(K_d)^2 - 8.85\,(K_d)^3 \qquad (2)$$

where MD is the mean diameter in nanometers.

Dynamic light scattering

The mean diameters of the initial vesicles were determined with a nanozizer apparatus (Coulter Electronics). For each sample three to four measurements have been performed to get an average value with a standard deviation smaller that 10%.

Fluorescence measurements

The fluorescence measurements were performed on a spectrofluorometer SPEX (F1L11I) connected to a computer.

For the solubilization experiments, the emission spectra of Laurdan (excitation wavelength (λ_{exc}) = 350 nm and 400 < emission wavelength (λ_{em}) < 550 nm) were recorded at 25°C during the continuous addition of detergent into a cuvette containing the initial vesicles at a precisely known concentration and under magnetic stirring. Considering that the cycle time (T_c) between two emission spectra is 140 s (96 s for the spectrum (T_s) and 44 s for the data transfer and monochromator movements), that the rate of detergent addition (r_s) is obtained from the total volume of the syringe (v_{ser}) and the time required to empty the syringe (T) ($r_s = v_{ser}/T$ in ml/min), and knowing precisely the initial concentration of the lipid in the cuvette ([Lip]$_o$ in mM), the initial volume of the vesicle solution (v_o in ml) and the detergent concentration in the syringe ([OG]$_s$ in mM), the data collected during the solubilization process were then treated to give for each point of the emission spectra the corresponding lipid and detergent concentrations using the following equations:

$$[OG]_{Tot} = ([OG]_s * r_s * t)/(v_o + r_s * t) \tag{3}$$

$$[Lip]_{Tot} = [Lip]_0/(1 + [OG]_{tot}/([OG]_s - [OG]_{tot})) \tag{4}$$

where [OG]$_{Tot}$ and [Lip]$_{Tot}$ are the total detergent and lipid concentrations in the cuvette and t the time (in minutes), which is deduced from each spectrum and each wavelength using the following equation:

$$t = T_c * (N_c - 1) + \frac{T_s * (\lambda - \lambda_{init})}{\lambda_{final} - \lambda_{init}} \tag{5}$$

where λ, λ_{init}, and λ_{final} are the running wavelength of the scan at time t, and the initial and the final wavelengths of the emission spectra recordings, respectively; N_c is the spectrum number.

Afterward, the ratio between the fluorescence intensity at the apparent maximum of the spectra and at 434 nm is plotted versus the total detergent concentration in the cuvette.

Moreover, we have ensured that no photobleaching or photooxydation of the probe occurs in our experimental conditions (one emission spectrum from 400 to 550 nm for λ_{exc} = 350 nm every 2 min, 20 s during 3 h). Indeed, after 3 h of exposure to incident 350 nm light, no significant variation of the fluorescence emission spectra of Laurdan in EPC/EPA small unilamellar vesicles (SUVs) was recorded.

EPC/EPA REVs containing NBD-PE and Rho-PE have also been used to follow the solubilization process induced by OG. Resonance energy transfer (RET) between NBD-PE and Rho-PE has been measured by following simultaneously the fluorescence intensity of NBD-PE (λ_{em} = 530 nm) and that of Rho-PE (λem = 590 nm) when the sample was excited at 470 nm, during the continuous addition of detergent into a cuvette containing the lipidic vesicles according to the experimental procedure described by Ollivon et al. (1988). The time was related to the lipid and detergent concentrations using Eqs. 3 and 4. The solubilization profiles were then obtained by plotting the ratio between the fluorescence intensities of NBD-PE and Rho-PE versus the total detergent concentration. For these experiments, we have used a mixture of unlabeled-labeled liposomes in a lipid ratio of 95/5 (M/M). These experimental conditions lead to a probe-to-lipid ratio of 0.1% (M/M) similar to the Laurdan-to-lipid ratio used in the other set of experiments.

Turbidity measurements

The solubilization of vesicles containing Laurdan was followed by measuring the turbidity at 550 nm (to avoid light absorption by Laurdan) during the continuous addition of the detergent to the quartz cuvette containing the lipidic vesicles. The measurements were performed on a Perkin-Elmer Lambda2 spectrophotometer connected to a computer. The data collected were treated afterward to relate the optical density (OD) to the real detergent and lipid concentrations by using Eqs. 3 and 4. The solubilization profiles are then obtained by plotting the OD at 550 nm versus the total detergent concentration.

RESULTS

Sensitivity of Laurdan to the vesicle-to-micelle transition

The normalized excitation and emission spectra of Laurdan incorporated in EPC/EPA REVs, mixed EPC-EPA-OG micelles, and pure OG micelles are presented in Fig. 1. In pure vesicles, the emission spectrum of Laurdan is asymmetrical and characterized by a maximum at 486 nm and a shoulder at about 434 nm. The addition to the vesicles of OG at concentrations higher than 7.75 mM induced a progressive shift of the maximum from 486 to 498 nm (Fig. 1, B and C). This red shift is relevant to an enrichment of the probe environment in OG, because Laurdan emission spectrum in pure OG micelles shows a maximum at 504 nm. Moreover, the intensity of the emission spectra decreased from the lamellar to the micellar structures. Fig. 1 C shows the
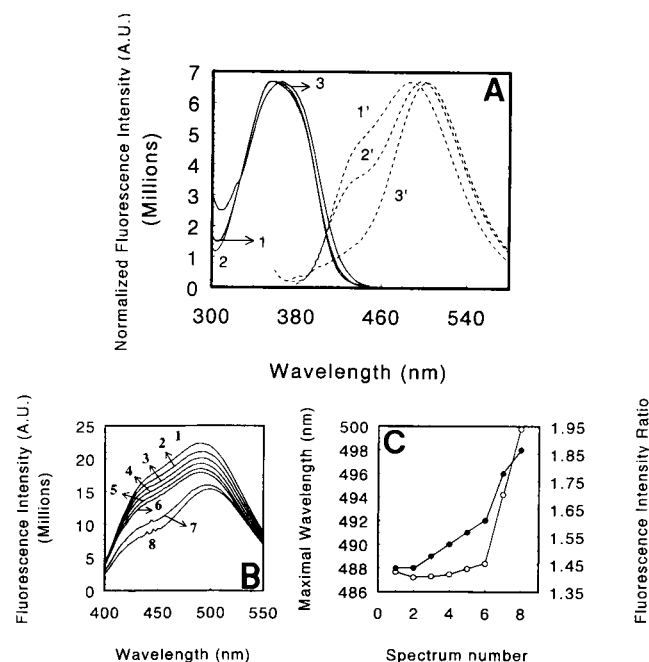

FIGURE 1 (A) Excitation (curves 1 to 3, λ_{em} = 490 nm) and emission (curves 1' to 3', λ_{exc} = 350 nm) spectra at 25°C of Laurdan ([Laur] = 1.8 μM) in EPC/EPA REV (90/10% M/M) ([Lip] = 1.2 mM) (curves 1, 1'), EPC/EPA/OG mixed micelles ([Lip] = 1.2 mM, [OG] = 25 mM) (curves 2, 2'), and pure OG micelles ([OG] = 200 mM) (curves 3, 3'). The spectra were corrected for instrument response and normalized at the excitation and emission maxima for each aggregate. (B) Emission spectra of Laurdan recorded during the solubilization of EPC/EPA REV ([Lip]$_0$ = 2.4 mM and [Laur]$_0$ = 3.6 μM) by OG (λ_{exc} = 350 nm). Spectra 1: [Lip] = 2.4 mM, [OG]$_{Tot}$ = 0 mM, 2: [Lip] = 2.35 mM, [OG]$_{Tot}$ = 4.0 mM, 3: [Lip] = 2.3 mM, [OG]$_{Tot}$ = 7.75 mM; 4: [Lip] = 2.25 mM, [OG]$_{Tot}$ = 11.45 mM; 5: [Lip] = 2.2 mM, [OG]$_{Tot}$ = 14.95 mM; 6: [Lip] = 2.15 mM, [OG]$_{Tot}$ = 18.3 mM; 7: [Lip] = 2.1 mM, [OG]$_{Tot}$ = 21.5 mM; 8: [Lip] = 2.05 mM, [OG]$_{Tot}$ = 24.6 mM. The emission spectra were corrected for the instrument response. The fluorescence intensities have been corrected from the dilution introduced by the addition of OG solution. (C) Evolution of the wavelength at the maximum of the emission spectra (●) and of the fluorescence intensity ratio (I_{max}/I_{434}) (○) as a function of the spectrum number in (B).

evolution of the fluorescence intensity ratio (I_{max}/I_{434}) during the solubilization process. As a function of OG content, below 7.75 mM the ratio decreases; then, after stabilization between 7.75 and 11.45 mM, the ratio significantly increases.

On the other hand, the emission spectra of Laurdan are sensitive to the energy of the excitation beam, as shown in Fig. 2 for Laurdan incorporated in EPC/EPA REVs, EPC/ EPA-OG mixed micelles, and OG pure micelles: when excited in the low energy part of the excitation spectrum $(\lambda_{exc} = 385$ nm and 410 nm), the shoulder observed in the emission spectra at about 434 nm tends to disappear, resulting in an increase of I_{max}/I_{434}.

Procedure for vesicle-to-micelle transition monitoring

The recorded fluorescence intensity of a probe is linearly related to its concentration as long as the inner filter effect
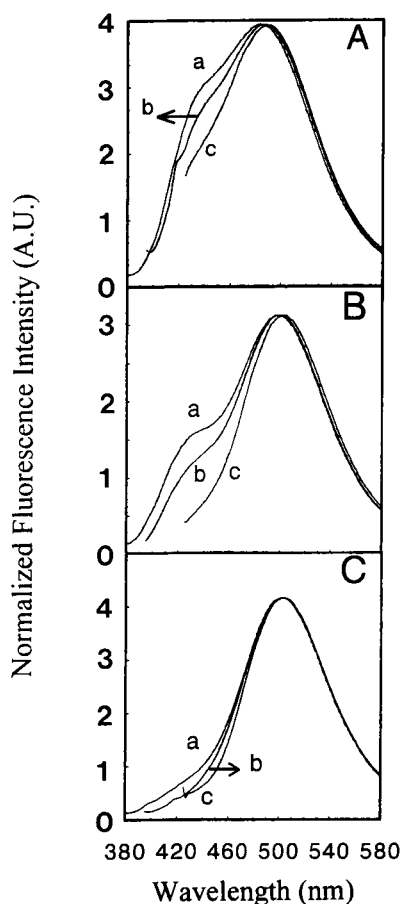

FIGURE 2 Effect of the excitation wavelength on the emission spectra of Laurdan incorporated in EPC/EPA REV ([Lip] = 1 mM, [Laur] = 1.5 μM) (A), EPC/EPA OG mixed micelles ([Lip] = 0.85 mM, [Laur] = 1.275 μM, [OG] = 28 mM) (B), and pure OG micelles ([Laur] = 1.64 μM, [OG] = 200 mM) (C). Emission spectra were recorded for an excitation wavelength of 350 (a), 385 (b), and 410 nm (c). All of the spectra were corrected from the instrument response. The spectra were also normalized to get an identical intensity at the maximum.

is negligible. The inner filter effect is due to the absorption of the excitation and emission light by the fluorophore but may also arise from light scattering, especially when the fluorescence measurements are performed on liposomal or micellar preparations. When the inner filter effect is no longer negligible, the experimental fluorescence intensity has to be corrected according to the following equation (Lakowicz, 1983):

$$\text{IF}_{cor} = \text{IF}_{exp} * 10^{((OD_{exc}+OD_{em})/2)} \qquad (6)$$

in which IF_{cor} and IF_{exp} are the corrected and experimental fluorescence intensities, respectively, and OD_{exc} and OD_{em} the optical densities at the excitation and at the emission wavelengths, respectively. To use the fluorescence of Laurdan to investigate the vesicle-to-micelle transition, a prerequisite was to set up the experimental conditions that minimize the inner filter effect and to find the fluorescence parameter that was affected as little as possible by it.

Pure OG micelles, mixed EPC-OG micelles, and EPC/ EPA REVs labeled with Laurdan were prepared at different compositions by varying the concentration of each constituent (probe, lipids, and detergent). The emission spectra of Laurdan incorporated into these three types of aggregates were recorded. In Table 1 are reported the concentration of each constituent, the experimental fluorescence intensities measured at 434 nm $(I_{434}exp)$ and at the maximum $(I_{max}exp)$ of the emission spectra, and the experimental fluorescence intensity ratio $([I_{max}/I_{434}]exp)$. From the experimental values, a linear relationship between the Laurdan concentration and the fluorescence intensities was obtained for probe concentrations ranging from 1 to 4 μM. However, if the fluorescence intensity ratio remains almost constant whatever the concentration of the constituent for a given aggregate, it changes from one aggregate to another: from 5.2 for pure micelles to 1.4 for EPC/EPA vesicles (Table 1).

To estimate the residual inner filter effect on the fluorescence intensity ratio and considering Eq. 6, we can write the equation of the corrected fluorescence intensity ratio $([\text{IF}_{max}/\text{IF}_{434}]cor)$:

$$\left[\frac{\text{IF}_{max}}{\text{IF}_{434}}\right]_{cor} = \left[\frac{\text{IF}_{max}}{\text{IF}_{434}}\right]_{exp} * 10^{\frac{OD_{max}-OD_{434}}{2}} \qquad (7)$$

This equation shows that the correction factor

$$10^{\left(\frac{OD_{max}-OD_{434}}{2}\right)}$$

is smaller than the one corresponding to the individual fluorescence intensities. The corrected intensities and ratios were calculated for all of the samples (Table 1). Linear relationships were obtained for low Laurdan concentrations (Table 1). From these equations, corrected fluorescence intensity ratios $([I_{434}/I_{max}]cor)$ were calculated for the higher concentrations. The results show that the residual systematic error due to the inner filter effect is about 1% in the experimental conditions used.

TABLE 1 Influence of the inner filter effect on the measured fluorescence parameters for different types of aggregates: pure OG micelles, mixed EPC/OG micelles, and EPC/EPA liposomes

Aggregate	[Laur] μM	[Lip] mM	[OG] mM	$I_{434\,exp}$ (A.U.)	$I_{max\,exp}$ (A.U.)	$[I_{max}/I_{434}]_{exp}$	Equations	$I_{434\,cor}$ (A.U.)	$I_{max\,cor}$ (A.U.)	$[I_{max}/I_{434}]_{cor}$	$\langle R_{exp}\rangle^a$	$\langle R_{cor}\rangle^b$
Pure micelles	0.51	—	200	0.75	3.91	5.18		0.75	3.92	5.19		
	1.02	—	200	1.51	7.82	5.18		1.51	7.81	5.185		
	4.05	—	200	5.14	26.74	5.20	$I_{434} = 1.5[Laur]$	5.99	31.04	5.18	5.19	5.18
	8.13	—	200	9.68	50.55	5.20	$I_{max} = 7.7[Laur]$	12.03	62.32	5.18		
	0.56	—	43	0.83	4.29	5.17		0.82	4.29	5.23		
	1.125	—	66	1.63	8.58	5.26		1.63	8.58	5.25	5.22	5.25
	2.25	—	110.5	3.13	16.48	5.26	$I_{434} = 1.45[Laur]$	3.26	17.16	5.26		
	4.5	—	200	5.78	30.06	5.20	$I_{max} = 7.6[Laur]$	6.52	34.22	5.26		
Mixed	0.56	0.375	18.85	2.93	5.85	2.00		2.98	6.11	2.05		
EPC/OG	1.12	0.75	19.9	5.97	12.25	2.05	$I_{434} = 5.3[Laur]$	5.97	12.25	2.05	2.02	2.05
micelles	2.25	1.5	22.0	10.92	22.04	2.02	$I_{max} = 10.9[Laur]$	11.94	24.50	2.05		
	4.5	3	26.2	19.47	39.00	2.00		23.88	49.00	2.05		
EPC/EPA	0.37	0.25	—	3.89	5.56	1.43		4.13	5.93	1.44		
REV	0.735	0.49	—	8.15	11.73	1.44		8.15	11.72	1.44		
(90/10)	1.46	0.975	—	14.21	20.18	1.42	$I_{434} = 11.1[Laur]$	16.21	23.32	1.44		
180 nm	2.26	1.505	—	20.76	29.06	1.40	$I_{max} = 15.9[Laur]$	25.02	36.01	1.44	1.41	1.44
	2.89	1.925	—	26.32	36.32	1.38		32.01	46.06	1.44		
	3.59	2.39	—	29.96	41.04	1.37		39.76	57.22	1.44		
	4.46	2.975	—	33.71	47.20	1.40		49.47	71.19	1.44		

$^a\langle R_{exp}\rangle$ = average $[I_{max}/I_{434}]_{exp}$
$^b\langle R_{cor}\rangle$ = average $[I_{max}/I_{434}]_{cor}$

In conclusion, within the precision obtained on the experimental ratio (about 1%), this last can be considered independent of the concentration of aggregates at a determined detergent and lipid composition and only related to the environment of the fluorophore for probe and lipid concentrations lower than 6 μM and 3 mM, respectively (Table 1).

Influence of the initial mean diameter of the vesicles on the solubilization process

The solubilization pathways of vesicles differing in their initial mean diameters were followed both at a supramolecular level by turbidity measurements and at a molecular level by Laurdan fluorescence measurements.

For this study it is necessary to get a series of vesicles of different sizes with strictly the same composition and sharp size distribution. It has been shown previously (Lesieur et al., 1991, 1993) that preformed EPC/EPA REVs successively extruded through Nucleopore filters with pore diameters from 0.8 to 0.05 μm were unilamellar and uniform in size and, moreover, kept a stable diameter for at least 1 month. Therefore an initial REV suspension was prepared by this procedure. Then this vesicle suspension was successively sonicated for 1 to 5 cycle(s) of 2 min duration to obtain five vesicle populations with sizes lower than the initial REVs.

The vesicles were characterized, according to Lesieur et al. (1993), by gel exclusion HPLC and quasi-elastic light-scattering measurements (data not shown). The agreement between the mean diameters of the liposomes obtained

for the six populations by these double analyses indicated the absence of aggregation. The size distribution of these EPC/EPA liposomes was analyzed by comparing the turbidity spectra at different elution volumes along the elution peak of the vesicles (data not shown). As these spectra are superimposed, it is reasonable to think that these liposomes are rather monodisperse (Lesieur et al., 1993).

The evolution of both turbidity at 550 nm and the fluorescence intensity ratio during solubilization by OG of Laurdan-labeled EPC/EPA vesicles ([Laur]/([Lip]) = 0.15% mole fraction), varying in initial size, is reported on Fig. 3. For each vesicle suspension, the initial lipid concentration was fixed at 0.5 mM. The experiments were monitored with the same rate of detergent addition (0.28 μmol OG/min) so that the composition of the successive aggregates formed during the solubilization process remained identical from one vesicle population to the other. The result is that the differences observed in turbidity (Fig. 3 A) and in Laurdan profiles (Fig. 3 B) were only related to the differences in the initial size of the liposomes.

The turbidity profiles are significantly different from one curve to the other. The most important changes appeared during the first part of the transition, which mainly corresponds to the insertion of the detergent molecules in the lipidic membrane before mixed micelle occurrence ([OG]$_{Tot}$ < 16.4 mM). The modifications observed are essentially related to differences in the supramolecular (size, shape, number, and refractive index of the mixed aggregates) events occurring during the solubilization process. The pathways became similar at the beginning of the micellization, i.e., at the appearance of the first mixed micelle event,

indicated by a white arrow on Fig. 3 A ($[OG]_{Tot} = 16.4$ mM). A common feature was that the onset (white arrow) and the end (black arrow; $[OG]_{Tot} = 18$ mM) of the solubilization process occurred in all cases at the same total OG concentration.

The solubilization profiles exhibited by the evolution of I_{max}/I_{434} (Fig. 3 B) were similar whatever the initial size of the vesicles, except at the initial step of OG insertion (for $0 < [OG]_{Tot} < 5$ mM). In this concentration range, the ratio varies with the size of the vesicles: the smaller the vesicles, the higher the ratio (Fig. 3 B, inset). In the 5–10 mM range for total OG concentrations, the ratio profiles slightly decrease whatever the initial size of the liposomes. For total OG concentrations ranging from 10 mM to the onset of the micellization process (17 mM), the ratio began to increase. The micellization process, i.e., between 16.4 and 18 mM, is characterized by a drastic increase of the ratio. After this domain, it continued to increase significantly but with a smaller slope (Fig. 3 B).
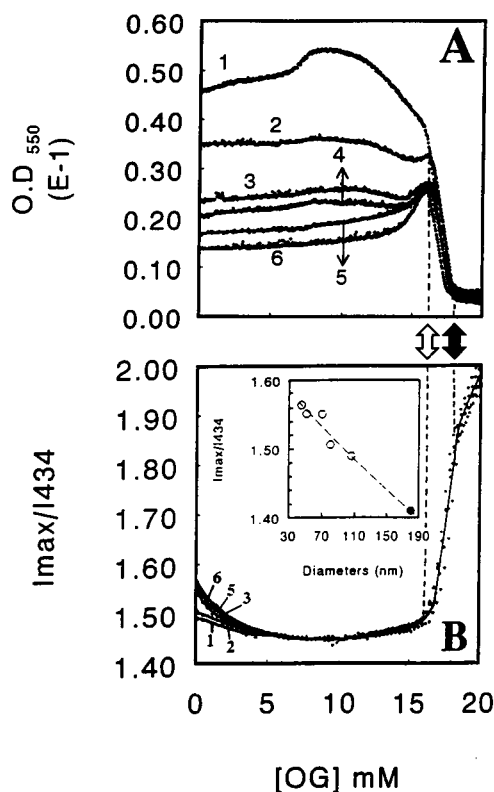
FIGURE 3　Evolution of the turbidity (A) and fluorescence intensity ratio (I_{max}/I_{434}) (B) during the solubilization by OG of EPC/EPA vesicle populations with decreasing sizes. The initial lipid concentration was fixed at 0.5 mM. The white and black arrows, respectively, indicate the beginning ($[OG] = 16.4$ mM) and the end ($[OG] = 18$ mM) of the micellization process. The mean gel exclusion HPLC diameters of the different vesicle suspensions are: 106 nm (curve 1), 80 nm (curve 2), 70 nm (curve 3), 65 nm (curve 4), 51 nm (curve 5), and 45 nm (curve 6). (Inset) Evolution of the fluorescence intensity ratio (I_{max}/I_{434}) versus the initial size of the vesicles: (O) vesicle populations corresponding to curves 1, 2, 3, 5, and 6. Also reported is the mean diameter of REV (●) used in Procedure for Vesicle-to-Micelle Transition Monitoring.

Partition coefficient determination

To determine the partition coefficient of OG between the solution and the aggregates two different set of experiments have been performed: one set using NBD-PE/Rho-PE-containing REVs and an another one using Laurdan-containing REVs.

The energy-transfer pair of lipid probes, NBD-PE and Rho-PE, has been previously used to follow the vesicle-to-micelle transition (Ollivon et al., 1988). Usually liposomes containing 1% (M/M) of each probe are used and the vesicle-to-micelle transition is revealed by the disappearance of RET. The evolution of the RET is measured by the fluorescence intensity ratio of the acceptor (Rho-PE) and of the donor (NBD-PE), i.e., the fluorescence intensity ratio I_{590}/I_{530}, when the sample is excited in the excitation spectra of the donor ($\lambda_{exc} = 470$ nm). However, in these experimental conditions the inner filter effect is not negligible, because of the high probe concentration. For this purpose, the experiments have been performed with a mixture of unlabeled and labeled liposomes in a lipid ratio of 95/5 (M/M), giving a probe-to-total lipid ratio of 0.1%, similar to the Laurdan-to-lipid ratio used for the other set of experiments. In these conditions the fluorescence intensity ratio I_{590}/I_{530} measured for the probes incorporated in the liposomes is constant in a range of total lipid concentration of 1 to 4 mM, corresponding to a total probe concentration of 1 to 4 μM (data not shown).

In Fig. 4 A, we have plotted the evolution of the fluorescence intensity ratio I_{590}/I_{530} versus the OG concentration for four different initial lipid concentrations (1, 2, 3, and 4 mM). The inset of Fig. 4 A shows two spectra corresponding to the probe inserted in liposomes (black line) and in mixed micelles (dashed line). The four solubilization profiles exhibit similar shapes; moreover, the I_{590}/I_{350} values are identical at the beginning and at the end of the curves independently on the initial lipid concentrations. This behavior allows the analysis of the experiment as indicated on Fig. 4 A. From the intercepts of isoratio horizontal lines with the experimental curves, OG concentrations ($[OG]_{Tot}$) were determined. Then the corresponding lipid concentrations ($[Lip]_{Tot}$) were calculated using Eq. 4, which takes into account the dilution factor introduced in the sample by the addition of OG solutions. $[OG]_{Tot}$ and $[Lip]_{Tot}$ obtained for each ratio value were plotted together (Fig. 4 B). The linear relationships relating both concentrations were fitted all along the domain of the transition studied (Ollivon et al., 1988; Lesieur et al., 1990):

$$[OG]_{Tot} = [OG]_{H_2O} + [OG/Lip]_{agg}[Lip]_{Tot} \qquad (8)$$

The OG-to-lipid concentration ratio in the aggregates ($R_a = [OG/Lip]_{agg}$) and the monomeric OG concentration in the aqueous phase ($[OG]_{H_2O}$), which is in equilibrium with the mixed aggregates, were deduced from the slopes and the origins of these straight lines, respectively. The analysis of the experiments has been performed for fluorescence intensity ratios ranging from 22 to 4.
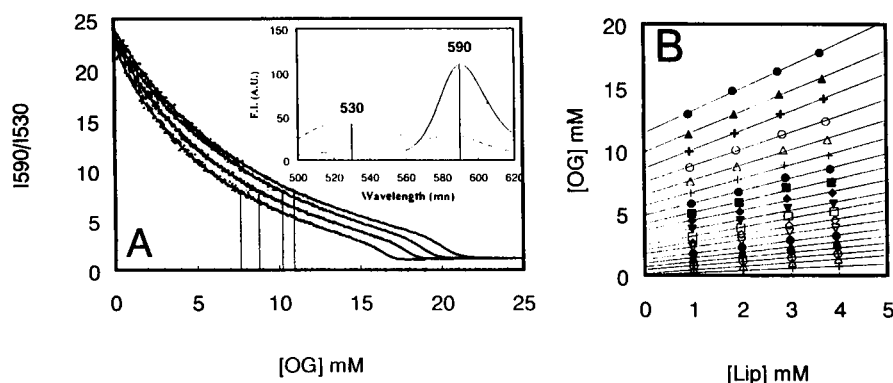
FIGURE 4 Solubilization by OG of mixture of 95/5% (M/M) of unlabeled/labeled EPC/EPA REVs with the transfer pair probes NBD-PE and Rho-PE and procedure for the determination of the partition coefficient K' of OG between amphiphilic and water phases. (A) Evolution of the fluorescence intensity ratio (I_{590}/I_{530}) when $\lambda_{exc} = 470$ nm of the sample during continuous addition of octylglucoside: for the curves from the left to the right $[Lip]_o = 1$ mM, $[Lip]_o = 2$ mM, $[Lip]_o = 3$ mM and $[Lip]_o = 4$ mM. The horizontal line indicates an isoratio; the intercept of this line with each of the four experimental curves allows the determination of OG concentrations. The lipid concentrations are then deduced from each OG concentration using Eq. 4 (Materials and Methods). This analysis has been done for isoratios ranging from 22 to 4. (B) The OG concentrations necessary to reach each of the fluorescence intensity ratio values analyzed versus the lipid concentration are plotted, and the linear relationships relating these points are determined. According to Eq. 8, the OG-to-lipid concentration ratios within the aggregates (R_a) and the monomer concentrations of OG $([OG]_{H_2O})$ are determined, respectively, from the slopes and the origins of these lines.

In Fig. 6, we plotted the evolution of the molar fraction of the detergent in mixed lipid-OG aggregates $(R_a/(R_a + 1))$ versus the monomeric detergent concentration $([OG]_{H_2O})$ obtained from NBD-PE/Rho-PE liposomes (open circles). This set of experiments gives the evolution of OG partitioning in the first part of the vesicle to micelle transition in which only vesicles exist.

Similarly, Laurdan-containing liposomes has been used to determine the partition of OG between the aggregates and the solution. Fig. 5, A and B, represents two sets of experiments that have been designed to have precision in the micellar part (Fig. 5 A) and in the vesicular part at the beginning of the transition (Fig. 5 B). As stated by the results of Table 1 and Fig. 1 C, each aggregation state of lipid and detergent occurring during the vesicle-to-micelle transition can be related to a given fluorescence intensity ratio within the precision of the experimental ratio. As a consequence, the ratio profiles were exploited between 1.44 and 3.8 in ratio (Fig. 5, A and B). The procedure of determination of OG and lipid concentrations corresponding to a given intensity ratio was similar to that developed for NBD-PE/Rho-PE-containing liposomes. Similarly again, we plot-
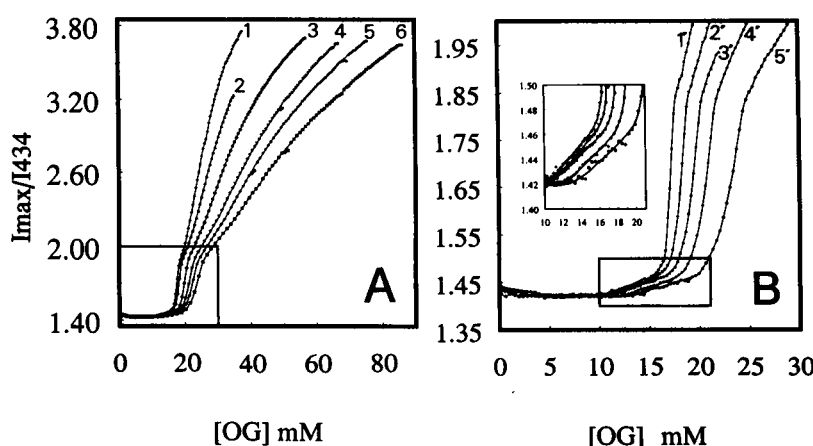

FIGURE 5 Solubilization by OG of Laurdan EPC/EPA REV. (A) Evolution of the fluorescence intensity ratio (I_{max}/I_{434}) of the emission spectra of Laurdan incorporated in EPC/EPA REVs during continuous addition of octylglucoside: $[Lip]_o = 0.5$ mM (trace 1), $[Lip]_o = 1$ mM (trace 2), $[Lip]_o = 1.5$ mM (trace 3) and $[Lip]_o = 2$ mM (trace 4), $[Lip]_o = 3$ mM (trace 5), $[Lip]_o = 3.5$ mM (trace 6). (B) Evolution of the fluorescence intensity ratio (I_{max}/I_{434}) of the emission spectra of Laurdan incorporated in EPC/EPA REV during continuous addition of octylglucoside: $[Lip]_o = 0.5$ mM (trace 1'), $[Lip]_o = 1$ mM (trace 2'), $[Lip]_o = 1.5$ mM (trace 3') and $[Lip]_o = 1.9$ mM (trace 4'), $[Lip]_o = 3$ mM (trace 5'). Different OG concentrations were used in the syringes in these two sets of experiments to get information about the transition in the micellar domain (A) or the vesicular and micellization domain (B). (Inset) Zoom of the previous curves on the domain delimited by the box in (B). The procedure used to determine the R_a and the corresponding $[OG]_{H_2O}$ was similar to the one described in Fig. 4. This analysis has been done for isoratios ranging from 1.43 to 3.8.

ted the evolution of the molar fraction of the detergent in mixed lipid-OG aggregates ($R_a/(R_a + 1)$)) versus the monomeric detergent concentration ($[OG]_{H_2O}$) obtained from Laurdan liposomes (Fig. 6, black circles). This set of experiments gives the evolution of the OG partition from the end of the vesicular part to the end of mixed-micellar part of the transition.

The curve of Fig. 6 represents the enrichment of the amphiphilic aggregates in OG during the vesicle-to-micelle transition. It presents five different domains: two in the lamellar part of the transition (for $0 < [OG]_{H_2O} < 15.6$ mM), one in the micellization part, and, finally, two in the
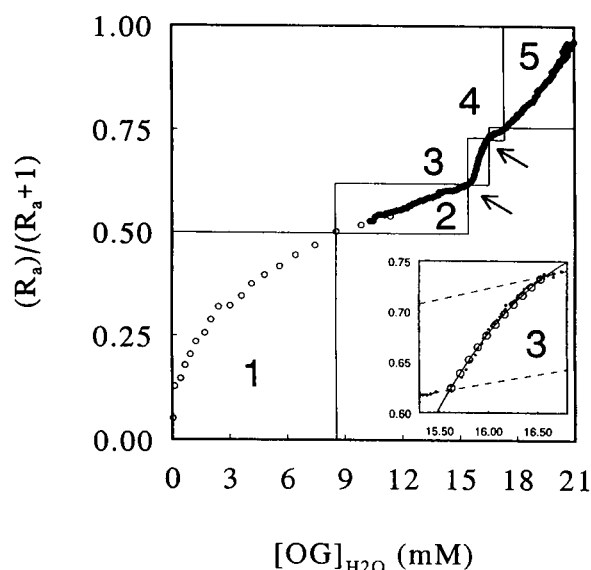

FIGURE 6 Variation of the molar fraction of OG in the aggregates versus the monomeric OG concentration in the continuous aqueous phase. O, data obtained from NBD-PE/Rho-PE fluorescence measurements; ●, data obtained from Laurdan fluorescence measurements. The two arrows indicate the onset ($R_a = 1.66$ and $[OG]_{H_2O} = 15.6$) and the end ($R_a = 2.74$ and $[OG]_{H_2O} = 16.5$) of the micellization process, which is defined by domain 3. (Inset) Zoom of the previous curve, on the region between the onset and the end of the micellization process (domain 3): ●, experimental points; O, calculated values according to the hypothesis that this intermediate domain is composed by the mixtures of the phases present at the limits of this domain. At the beginning of this domain (lipid-rich limit), the composition of the aggregates is determined by a detergent-to-lipid concentration ratio (R_{a1}) of 1.66 in equilibrium with a detergent monomeric concentration ($[OG]_{H_2O_1}$) of 15.6 mM. At the end of this domain (detergent-rich limit), the composition of the aggregates is determined by a detergent-to-lipid concentration ratio (R_{a3}) of 2.74 in equilibrium with a detergent monomeric concentration ($[OG]_{H_2O_2}$) of 16.5 mM. Caculated detergent molar fractions ($(R_a/(R_a + 1))_{calc}$) and caculated monomeric OG concentrations ($([OG]_{H_2O})_{calc}$) were obtained from the following equations:

$$\left(\frac{R_a}{R_a + 1}\right)_{calc} = \frac{\alpha R_{a1} + (1 - \alpha)R_{a3}}{1 + \alpha R_{a1} + (1 - \alpha)R_{a3}} \qquad (15)$$

$$([OG]_{H_2O})_{calc} = \alpha[OG]_{H_2O_1} + (1 - \alpha)[OG]_{H_2O_2} \qquad (16)$$

where α varies from 1 to zero (0.1 steps) from the onset to the end of the micellization process.

pure micellar part (for $16.5 < [OG]_{H_2O} < 21$ mM). In two of these domains (noted 2 and 4), the experimental points are fitted by linear relationships, whereas in the other three domains the experimental points cannot be fitted by simple relationships (see Discussion).

DISCUSSION

Evolution of the emission spectra of Laurdan during the solubilization process

We have demonstrated (Figs. 1 and 2) that the emission spectra of Laurdan are sensitive to the vesicle-to-micelle transition, i.e., during the transition the intensity of the emission spectrum gradually decreases, the maximal component of the emission spectrum is red shifted, and, finally, the fluorescence intensity ratio I_{434}/I_{max} is changing.·Moreover, the data of Table 1 show that the fluorescence intensity ratio, experimentally determined from the emission spectrum obtained for Laurdan incorporated in EPC/EPA (90/10 M/M) liposomes, mixed OG/EPC/EPA micelles, and pure OG micelles is only dependent on the environment of the probe in the experimental conditions chosen in this work.

The photochemical origin of the spectral changes occurring during the solubilization process is not elucidated. It is known that at the excited state the Laurdan has a very large dipole that can react with the surrounding solvent molecules. As the fluorophore is probably located at the hydrophobic-hydrophilic interface, the relaxation process occurring at the membrane-water interface or at the micelle-water interface may be very different because of the different packing of the aggregates. However, to understand the photophysics of the probe, experiments must be undertaken, and in particular, fluorescence time-resolved spectra must be determined.

The vesicle-to-micelle transition: influence of the initial size of the vesicles on the solubilization pathway

The turbidity curves obtained for the solubilization of monodisperse populations of unilamellar vesicles with identical composition and concentration, but different initial sizes, show drastic differences. Indeed, turbidity is related to size, shape, possible aggregation, concentration, and relative refractive index of the aggregates (Lesieur et al., 1993). All of these parameters depend in turn on the insertion of OG into the bilayer and its consequences for the membrane thickness and the volume occupied by the lipidic shell.

The fact that up to the beginning of the micellization, the turbidity recordings versus vesicle size are different indicates that the initial size is a preponderant factor in the evolution of the aggregates along the lamellar part of the solubilization process. Moreover, the amplitude of the OD differences observed between the smaller and the larger aggregates indicates that up to at least $[OG]_{Tot} = 14$ mM

they probably are large aggregates—large initial vesicles yielding large aggregates and reciprocally smaller initial vesicles forming small aggregates. However, in the range of 5 mM < $[OG]_{Tot}$ < 14 mM, two different behaviors are observed, depending on the initial vesicle sizes. For the "large" vesicles (65 nm $\leq$ initial mean diameter $\leq$ 106 nm) the turbidity profiles are characterized by an initial slight increase followed by a bump, the amplitude of which is related to the initial size: the larger the size, the more important the amplitude of the bump. For the "small" vesicles (45 nm $\leq$ initial mean diameter $\leq$ 51 nm) the turbidity profiles are characterized by a continuous and slight increase. This turbidity increase has been interpreted by Ollivon et al. (1988) as vesicle swelling induced by OG insertion. On the contrary, the bump observed for large vesicles may be attributed to important changes in the morphology of the vesicles. Indeed, Vinson et al. (1989) have observed by cryotransmission electron microscopy that EPC vesicles of about 150 nm initial diameter were going from a spherical to mainly elongated cylindrical shape. Lasch et al. (1990) have proposed, according to the theory of Israelachvili (1985), that, because of membrane packing considerations, the incorporation of detergent molecules would stabilize the small vesicles more than the big ones. Indeed, because of the high curvature radius of the small vesicles, some spaces on the membrane surface are available for detergent incorporation, whereas fewer defects are present on the large vesicles, so that the incorporation of detergent molecules may result in important morphological changes of the lipid-detergent mixed vesicles compared to the initial ones.

At the molecular level, the Laurdan fluorescence profiles (Fig. 2 B) show that in the very first part of the solubilization process (0 < $[OG]_{Tot}$ < 5 mM), the decrease of the fluorescence intensity ratio depends on the initial size of the vesicles, but at $[OG]_{Tot}$ = 5 mM, it reaches a value of 1.45, whatever the initial size. This result indicates that Laurdan is sensitive to the local curvature radius, perhaps via the local molecular packing of the amphiphilic molecules constituting the aggregates. However, for $[OG]_{Tot}$ = 5 mM, the unique fluorescence intensity ratio depicted by all of the curves reflects the fact that the lipid and detergent packing becomes similar and independent of the mixed aggregate morphology. To maintain such a molecular packing, the different vesicle populations have to adapt their local curvature, leading to supramolecular rearrangements depending on the initial size, as illustrated by the turbidity curves (Fig. 2 A).

Interestingly, for the four vesicle size populations ranging from 45 to 70 nm, the turbidity observed between 14 and 17 mM in total OG concentration (Fig. 2 A) increases to the same OD value (0.028), indicating that the mixed vesicles adopt a definite structure that is similar in shape, size, and molecular organization. On the other hand, for the vesicles ranging from 80 to 106 nm in diameter, although the turbidity decreases, the critical OD value of 0.028 is not reached at the onset of the micellization process. Simulta-

neously, the fluorescence intensity ratio curves, which only depend on the detergent insertion in the bilayer and do not reflect the supramolecular arrangements, are superimposed whatever the initial size of the liposomes. Both observations (fluorescence and turbidity) strongly suggest that, in the case of large initial vesicles, the aggregate evolution is governed by slower processes at the time scale of the experiments. Indeed, the existence of an equilibrium size has been previously suggested for the OG-EPC system for which the rate of the detergent partition between the water and the lipidic phase is fast (Ollivon et al., 1988). These authors have shown, on EPC SUVs of 23 nm initial diameter, a growth to 61 nm after exposure to an OG concentration corresponding to the onset of the micellization process. Vinson et al. (1989) have similarly found that big unilamellar vesicles of 150 nm exposed to OG decrease to a size of 67 nm. On the other hand, exposure of EPC/EPA REVs to a similar OG concentration and after detergent removal by direct contact with Bio Beads SM2 leads to a size decrease of the liposomes from 110 $\pm$ 40 nm (initial REV size) to 70 $\pm$ 15 nm (Paternostre et al., 1988). Thus, these literature data are already consistent with an equilibrium size centered at about 65 nm. Our work suggests that this equilibrium size is reached, both at the molecular and the supramolecular level, at the onset of the solubilization process. Mechanisms based on either aggregation/fusion (Ollivon et al., 1988; Edwards et al., 1989) or lipid transfer (Almog et al., 1990) have been proposed to explain the growth of SUVs. On the contrary, no mechanisms have been proposed for the size reduction observed for large vesicles. An "exocytosis" mechanism involving membrane fusion may be invoked for the process by which large mixed vesicles collapse into smaller ones.

Beyond 17 mM in total OG concentration (Fig. 2), the evolution of the turbidity, as well as that of the fluorescence intensity ratio shows that the micellization process follows an identical pathway whatever the initial size of the liposomes. This behavior is effectively expected if an equilibrium state is reached at the onset of the process.

Partition coefficients

The fluorescence study of the solubilization of monodisperse unilamellar EPC/EPA REVs loaded with NBD-PE/Rho-PE on one hand and Laurdan on the other, at different lipid concentrations, made it possible to determine the OG-to-lipid molar ratio in the aggregates (R_a) and the OG concentration in the aqueous medium ($[OG]_{H_2O}$).

For the solubilization experiments performed on NBD-PE/Rho-PE REVs we used solutions containing a 5/95 ratio of labeled-unlabeled liposomes to reduce as much as possible the inner filter effect. The solubilization profiles obtained from the plot of I_{590}/I_{530} versus the OG concentration (Fig. 4) are rather different from those determined from the solubilization of pure labeled liposomes (Ollivon et al., 1988). Indeed, in this last case, a RET decrease of only a

few percent is recorded during the vesicular part of the transition, whereas in the experiments presented here, almost 100% RET decrease is recorded before the beginning of the solubilization. Ollivon et al. (1988) have already observed such behavior when 90% of the labeled SUVs where replaced by unlabeled ones (95% in our case) and demonstrated that the RET decrease is still relative to OG interaction with liposomes. The enhancement of RET decrease in the vesicular part of the transition, when mixtures of labeled and unlabeled liposomes are used, allows the exploitation of the curves with very good accuracy from the very beginning of the vesicular part of the transition.

The plot of $R_a/(R_a + 1)$ versus $[OG]_{H_2O}$ throughout the solubilization process (Fig. 6) describes a curve that is not linear but presents five different domains, and for at least two of them, the experimental points fit a linear relationship. This means that the detergent partition coefficient changes throughout the vesicle-to-micelle transition.

The partition behavior of OG between the aqueous medium and EPC SUVs was studied by Ueno (1989) and Almog et al. (1990), using dialysis and ultracentrifugation, respectively. Almog et al. (1990) determined a unique partition coefficient (33 M^{-1}) for the detergent over the entire transition. On the contrary, Ueno (1989) has obtained a curve for the plot of $R_a/(R_a + 1)$ versus $[OG]_{H_2O}$, which looks like the one reported on Fig. 6. By applying Eq. 14, he calculated $((R_a/(R_a + 1))/[OG]_{H_2O})$, which represents K', and from the plot of K' versus $[OG]_{H_2O}$ he revealed two domains: one delimited by $0 < [OG]_{H_2O} < 4.4$ mM and $0 < R_a < 0.43$, for which K' is constant to about 75 M^{-1}, and one for which K' is continuously changing until the end of the solubilization process.

The linear law described by Eq. 14 can only be obtained for a two-phase domain and only if the structural properties of the two phases remain unaffected by increasing the concentration of the external molecule partitioning between them.

The vesicle-to-micelle transition, induced by the addition of OG molecules, is characterized by a structural change from a two-phase domain (vesicles and water) to a one-phase domain (aqueous micellar solution) via successive steps that can correspond to intermediate phase transitions. The curve presented in Fig. 6 can be described by five distinct domains. The two linear domains (domains 2 and 4 in Fig. 6) successively detected during the solubilization process are consistent with the presence of distinct two-phase domains. Each of these domains is defined by a specific constant partition coefficient determined by the slope of the straight lines: 18.2 M^{-1} and 21 M^{-1} for domains 2 and 4, respectively.

The molar fraction of OG in the lipidic matrix obtained for the very beginning of the transition (domain 1) were not linearly related to the OG concentration in water. Moreover, this domain is characterized by a continuous decrease of the partition coefficient of OG. In domain 2, the partition coefficient of OG is constant and the affinity of OG molecules for this "mixed membrane" is strongly reduced compared to the one for the pure phospholipidic membrane present at the beginning of domain 1. These two partitioning behaviors of OG in the vesicular part of the transition imply a rearrangement of the lipid and the detergent organization in the bilayer.

Our data can be compared with small-angle x-ray scattering (SAXS) data obtained by Beugin et al. (1995) on EPC/OG system. The experiments have been performed on concentrated multilayers of EPC (about 700 mM) with increasing concentrations of OG. SAXS patterns have been recorded as a function of the total OG/Lip ratios. It is worth noting that the total OG/Lip ratios are close to the effective OG/Lip ratio in the membrane because the samples are very concentrated and the $[OG]_{H_2O}$ is negligible. These ratios are then fully comparable to the R_a measured in our study. For total OG/Lip ratios ranging from 0.1 to 0.71, i.e., the ratios reached in the domain 1 of Fig. 6, the SAXS patterns show complex diffraction peaks from which at least two lamellar distances can be determined: one at about 64 Å and an another one at about 57 Å. These long spacings may correspond to the thickness of the pure EPC lamellae and a "mixed lamellae," respectively. This phase diagram region is reflected by continuous evolution of the partition of detergent between the aqueous phase and the lipids (Fig. 6, Domain 1). Both SAXS (Beugin et al., 1995) and fluorescence (this work) studies suggest that more than two phases may be present in this domain (multiple repeat distances and partition coefficient not constant), providing both studies have been performed in equilibrium conditions. For OG/Lip ratios ranging from 0.99 to 1.53, i.e., the limit ratios reached in domain 2, a single set of sharp lamellar long spacings is observed and corresponds to a repeat distance of about 62 Å intermediate between the preceding values. For these last ratios, a homogeneous "detergent-rich" lamellar phase is detected that corresponds to a nearly constant partition coefficient, as expected for a biphasic system (here, water and lamellar phase) (domain 2, Fig. 6).

Then, the vesicular part of the transition can then be interpreted as the transformation of the pure phospholipidic lamellar phase (pure vesicles without any OG) into a "detergent-rich" one (domain 2). This transformation is realized during the intermediate domain 1. Indeed, Beugin et al. (1995) visualized this structural transformation for OG/Lip ratios, which are comparable to ours.

Between the onset and the end of the solubilization process (domain 3), the experimental points do not describe a linear law. From previous observations and by different techniques (quasi-elastic light scattering: Edwards et al., 1989; nuclear magnetic resonance: Jackson et al., 1982; Paternostre et al., 1988; turbidity: Ollivon et al., 1988) it turns out that two types of aggregates, lamellar and micellar, coexist in this domain. Moreover, it has also been shown, by ultracentrifugation separation technique and for the solubilization of EPC/EPA REVs by octaethylene glycol mono-n-dodecyl ether (another non-ionic detergent) (Lévy et al., 1990), that, in the region of the micellization process, the relative composition in lipid and detergent of the superna-

tant (micellar aggregates) and that of the pellet (vesicular aggregates) remain constant. From our work, we have shown that this domain is located between two two-phase domains (domains 2 and 4). In terms of phase behavior the system necessarily passes through a three-phase domain in which OG partitions between the two types of aggregates and water. Indeed, the experimental points fit the partitioning law of detergent established by Eqs. 15 and 16, based on this assumption (Fig. 6, inset).

In the micellar part of the transition, two distinct domains of detergent partitioning are determined: in the first one (domain 4) the experimental points fit a linear relationship that corresponds to a partition coefficient of 21 M^{-1}, whereas in the second one (domain 5) the experimental points describe a nonlinear curve that tends toward the value 1/(critical micellar concentration) (1/CMC) when the molar fraction of detergent in the mixed micelles tends to 1 (Fig. 6). The existence of these two distinct detergent partitioning laws in the mixed-micellar domains has never been observed,either because of an insufficient number of experimental points (Ueno, 1989) or because the detergent and lipid concentration range explored only corresponds to domain 5 (Eidelman et al., 1988). However, in this last work, the results show a noticeable discrepancy with our data. This can be explained by the very high concentration (2% to 6% in mole fraction) of NBD-PE and Rho-PE used for RET experiments, which may change the characteristics of the bilayers.

Vinson et al. (1989), by cryotransmission electron microscopy of the EPC/OG system, have seen the presence of long cylindrical micelles up to a R_a of 3, whereas for higher R_a in the aggregates, they have only detected small spheroidal micelles. These structural changes can be related to the rupture between the two domains 4 and 5, which occurs at a R_a value of 3.13. For $2.74 < R_a < 3.13$, and because the experimental points fit a linear relationship, the domain can be composed of two phases, i.e., the aqueous phase and a micellar one that could correspond to the long cylindrical micelles as observed by Vinson et al. (1989). For domain 5, the molar fraction of OG in the aggregates is not linearly related to $[OG]_{H_2O}$. For $R_a > 3.13$, and again according to the pictures shown by Vinson et al. (1989), the micelles are small and are not in interaction. If such a micellar domain can be represented as a one-phase domain, Eq. 14 would no longer be valid. The experimental points may be then related to an association equilibrium of detergent and lipid forming mixed micellar aggregates.

Finally, the monomeric detergent concentration continuously increases (from 0 to almost 21 mM) throughout the solubilization process. This observation is consistent with different work performed on liposome solubilization by OG (Ueno, 1989; Lesieur et al., 1990; Seras et al., 1992, 1993). Although the amount of phospholipid molecules dissolved in water is very low, it could have a direct influence on the detergent CMC. Indeed, according to Tanford (1980), the mixture of two amphiphilic compounds induces the lowering of their CMCs, the value of which depends on the molar

ratio of both compounds. This would explain the fact that the monomeric OG concentration in equilibrium with the mixed aggregates is always lower than its CMC and is changing throughout the vesicle-to-micelle transition, tending toward 21 mM, i.e., the OG CMC in our buffer, when the molar fraction of OG tends to 1 (see Fig. 6).

In conclusion, the use of Laurdan for the study of the vesicular-to-micellar transition gives interesting and new information about the molecular and supramolecular events of the solubilization pathway. *First*, the combination of turbidity and fluorescence measurements points out the existence of a unique vesicular state at the onset of the micellization that is identical regarding the size, shape, and molecular organization, whatever the initial size of the vesicles. This strongly supports the idea of the formation of an equilibrium size of the vesicles connected to the relation between the curvature radius and the detergent and lipid composition of the vesicles. *Second*, the use of NBD-PE and Rho-PE on one hand and of Laurdan on the other allows the continuous determination of the detergent partitioning throughout the solubilization process and, moreover, avoids long and tedious lipid and detergent assays. It is important to emphasize that these probes can be applied to the determination of the partition of any amphiphilic molecule between water and membranes. This methodology represents a powerful tool for monitoring membrane protein incorporation into liposomes. *Third*, the analysis of the partition behavior of the detergent leads to the accurate description of the phase domains appearing during the vesicle-to-micelle transition. The transition goes from a two-phase domain (vesicular and aqueous phases) to a one-phase domain (mixed micellar solution), passing through a succession of five intermediate domains. In particular, the change of the detergent partition behavior in the vesicular region of the transition strongly suggests the existence of two distinct lamellar structures (the pure phospholipidic bilayer (EPC/EPA) and a "detergent-rich lamellar" phase (domain 2) separated by an intermediate domain (domain 1). The micellization process agrees with a model of a three-phase domain composed of detergent-saturated lamellae, lipid-saturated mixed micelles, and aqueous medium. A small two-phase domain has been delimited in the micellar region near the end of the solubilization process, followed by a domain for which the molar fraction of the detergent in the aggregates is not linearly related to $[OG]_{H_2O}$.

This work, as a whole, represents an essential approach to lipid and detergent phase behavior and gives at the molecular level the boundaries of each phase domain. This is also the basis for further structural investigations that are required to fully understand the mechanisms of the solubilization process. On the other hand, because of the very high sensitivity of Laurdan to its environment, the photophysics of the probe itself is far from being entirely elucidated. To totally interpret the information we get with this probe, time-resolved fluorescence experiments are being undertaken.

APPENDIX

The partition coefficient K of OG between two non-miscible phases (lipidic and aqueous phases) is defined by the following equation (Jackson et al., 1982):

$$K = (X_{OG/Lip})/(X_{OG/H2O}) \qquad (9)$$

in which $X_{OG/lip}$ and $X_{OG/H2O}$ are the molar fractions of OG in the lipidic and aqueous phases, respectively. These molar fractions are defined as follows:

$$X_{OG/Lip} = [OG]_{Lip}/([OG]_{Lip} + [Lip]) \qquad (10)$$

$$X_{OG/H2O} = [OG]_{H2O}/([OG]_{H2O} + [H_2O]) \qquad (11)$$

in which $[OG]_{lip}$ and $[OG]_{H2O}$ are the OG concentrations in the lipidic aggregates and water, respectively, and [Lip] and $[H_2O]$ are the total lipid and H_2O concentrations, respectively.

$X_{OG/lip}$ can be expressed as a function of the detergent-to-lipid molar ratios in the aggregates R_a using Eq. 12:

$$X_{OG/Lip} = R_a/(R_a + 1) \qquad (12)$$

In the denominator of Eq. 10, considering the low solubility of OG monomers in water, $[OG]_{H2O}$ can be neglected in front of $[H_2O]$, and Eq. 9 may be simplified:

$$K \approx (R_a/(R_a + 1)) * ([H_2O]/[OG]_{H2O}) \qquad (13)$$

Finally, Eq. 14 defines the partition coefficient K', which is often used in practice (Jackson et al., 1982):

$$K' = K/[H_2O] \text{ in } M^{-1} \qquad (14)$$

K' is also directly related to R_a and $[OG]_{H2O}$ as follows:

$$(R_a/(R_a + 1)) = K'([OG]_{H2O}) \qquad (15)$$

It is worth noting that Eq. 15 is only valid for a two-phase domain. Moreover, K' is constant only if the nature of these two phases (amphiphilic and aqueous) remains unchanged throughout the detergent addition.

REFERENCES

Almog, S., B. J. Litman, W. Wimley, J. Cohen, E. J. Wachtel, Y. Barenholz, A. Ben-Shaul, and D. Lichtenberg. 1990. States of aggregation and phase transformation in mixtures of phosphatidylcholine and octyl glucoside. *Biochemistry.* 29:4582–4592.

Beugin, S., C. Grabielle-Madelmont, M. Paternostre, M. Ollivon, and S. Lesieur. 1995. Phosphatidylcholine vesicle solubilization by glucosidic non-ionic surfactants: a turbidity and x-ray diffraction study. *Prog. Colloid Polym. Sci.* 98:206–211.

Chong, P. L.-G. 1988. Effects of hydrostatic pressure on the location of PRODAN in lipid bilayers and cellular membranes. *Biochemistry.* 27: 399–404.

Chong, P. L.-G., S. Capes, and P. T. T. Wong. 1989. Effects of hydrostatic pressure on the location of PRODAN in lipid bilayers: a FT-IR study. *Biochemistry.* 28:8358–8363.

Conrad, M. J., and S. J. Singer. 1981. The solubility of amphipathic molecules in biological membranes and lipid bilayers and its implications for membrane structure. *Biochemistry.* 20:808–818.

Cowley, D. J. 1986. Polar pocket with nonpolar lining. *Nature.* 319:14–15.

da Graça Miguel, M., O. Eidelman, M. Ollivon, and A. Walter. 1989. Temperature dependence of the vesicle-micelle transition of egg phosphatidylcholine and octyl glucoside. *Biochemistry.* 28:8921–8928.

de Foresta, B., Z. Merah, M. le Maire, and B. Champeil. 1990. How to evaluate the distribution of an "invisible" amphiphile between biological membranes and water. *Anal. Biochem.* 189:59–67.

del Rio, E., J. M. Gonzalez-Manas, J.-I. G. Gurtubay, and F. M. Goni. 1991. On the mechanism of bacteriorhodopsin solubilization by surfactants. *Arch. Biochem. Biophys.* 291:300–306.

Edwards, K., M. Almgren, J. Bellare, and W. Brown. 1989. Effects of Triton X-100 on sonicated lecithin vesicles. *Langmuir.* 5:473–478.

Eidelman, O., R. Blumenthal, and A. Walter. 1988. Composition of octyl glucoside-phosphatidylcholine mixed micelles. *Biochemistry.* 27: 2839–2846.

Inoue, T., T. Yamahata, and R. Shimozawa. 1992. Systematic study on the solubilization of phospholipid vesicles by various surfactants. *J. Colloid Interface Sci.* 149:345–358.

Israelachvili, J. N. 1985. Thermodynamic and geometric aspects of amphiphile aggregation into micelles, vesicles and bilayers and the interaction between them. *In* The Proceedings of the "Scuola Internazionale di Fisica "Enrico Fermi," XC Corso, Fisica degli amfifili: micelle, vesicole e microemulioni. V. Degiorgio, editor. North-Holland Physics Publishing, Amsterdam. 24–58.

Jackson, M. L., C. F. Schmidt, D. Lichtenberg, B. J. Litman, and A. D. Albert. 1982. Solubilization of phosphatidylcholine bilayers by octyl glucoside. *Biochemistry.* 21:4576–4582.

Kragh-Hansen, U., M. le Maire, J.-P. Noël, T. Gulik-Krzywicki, and J. V. Moller. 1993. Transitional steps in the solubilization of protein-containing membranes and liposomes by nonionic detergent. *Biochemistry.* 32:1648–1656.

Lakowicz, J. R. 1983. Mechanisms and dynamics of solvent relaxation. *In* Principles of Fluorescence Spectroscopy. J. R. Lackowicz, editor. Plenum Press, New York and London. 189–215.

Lasch, J., J. Hoffman, W. G. Omelyanenko, A. A. Klibanov, V. P. Torchilin, H. Binder, and K. Gawrisch. 1990. Interaction of Triton X-100 and octyl glucoside with liposomal membranes at sublytic and lytic concentrations. Spectroscopic studies. *Biochim. Biophys. Acta.* 1022:171–180.

le Maire, M., J. V. Moller, and P. Champeil. 1987. Binding of a nonionic detergent to membranes: flip-flop rate and location on the bilayer. *Biochemistry.* 26:4803–4810.

Lesieur, S., C. Grabielle-Madelmont, M. Paternostre, J. M. Moreau, R. M. Handjani-Villa, and M. Ollivon. 1990. Action of octylglucoside on non-ionic monoalkyl amphiphile-cholesterol vesicles: study of the solubilization mechanism. *Chem. Phys. Lipids.* 56:109–121.

Lesieur, S., C. Grabielle-Madelmont, M. Paternostre, and M. Ollivon. 1991. Size analysis and stability study of lipid vesicles by high-performance gel exclusion chromatography, turbidity, and dynamic light scattering. *Anal. Biochem.* 192:334–343.

Lesieur, S., C. Grabielle-Madelmont, M. Paternostre, and M. Ollivon. 1993. Study of size distribution and stability of liposomes by high performance gel exclusion chromatography. *Chem. Phys. Lipids.* 64: 57–82.

Lévy, D., A. Gulick, M. Seigneuret, and J.-L. Rigaud. 1990. Phospholipid vesicle solubilization and reconstitution by detergents. Symmetrical analysis of the two processes using octaethylene glycol mono-*n*-dodecyl ether. *Biochemistry.* 29:9480–9488.

Lichtenberg, D., and Y. Barenholz. 1988. Liposomes: preparation, characterization and preservation. *Methods Biochem. Anal.* 33:337–367.

Livesey, A. L., and J. C. Brochon. 1987. Analyzing the distribution of decay constants in pulse-fluorimetry using the maximum entropy method. *Biophys. J.* 52:693–706.

McClure, W. O., and G. M. Edelman. 1966. Fluorescent probes for conformational states of proteins. I. Mechanism of fluorescence of 2-*p*-toluidinylnaphtalene-6-sulfonate, a hydrophobis probe. *Biochemistry.* 5:1908–1918.

Macgregor, R. B., and G. Weber. 1981. Fluorophores in polar media: spectral effects of the Langevin distribution of electrostatic interactions. *Ann. NY Acad. Sci.* 366:140–154.

Macgregor, R. B., and G. Weber. 1986. Estimation of the polarity of the protein interior by optical spectroscopy. *Nature.* 319:70–73.

Meyer, O., M. Ollivon, and M. Paternostre. 1992. Solubilization steps of dark-adapted purple membrane by Triton X-100. A spectroscopic study. *FEBS Lett.* 305:249–253.

Ollivon, M., O. Eidelman, R. Blumenthal, and A. Walter. 1988. Micelle-vesicle transition of egg phosphatidylcholine and octyl glucoside. *Biochemistry.* 27:1695–1703.

Ollivon, M., A. Walter, and R. Blumenthal. 1986. Sizing and separation of liposomes, biological vesicles and viruses by high-performance liquid chromatography. *Anal. Biochem.* 152:262–274.

Parasassi, T., F. Conti, and E. Gratton. 1986. Time-resolved fluorescence emission spectra of laurdan in phospholipid vesicles by multifrequency phase and modulation fluorometry. *Cell. Mol. Biol.* 32:103–108.

Parasassi, T., G. De Satasio, A. d'Ubaldo, and E. Gratton. 1990. Phase fluctuation in phospholipid membranes revealed by laurdan fluorescence. *Biophys. J.* 57:1179–1186.

Parasassi, T., G. De Satasio, G. Ravagnan, R. M. Rush, and E. Gratton. 1991. Quantitation of lipid phase in phospholipid vesicles by the generalized polarization of laurdan fluorescence. *Biophys. J.* 60:179–189.

Parasassi, T., M. Di Stefano, M. Loiero, G. Ravagnan, and E. Gratton. 1994. Influence of cholesterol on phospholipid bilayers phase domains as detected by laurdan fluorescence. *Biophys. J.* 66:120–132.

Parasassi, T., and E. Gratton. 1992. Packing of phospholipid vesicles studied by oxygen quenching of laurdan fluorescence. *J. Fluorescence.* 2:167–174.

Paternostre, M., M. Roux, and J.-L. Rigaud. 1988. Mechanisms of membrane protein insertion into liposomes during reconstitution procedures involving the use of detergents. 1. Solubilization of large unilamellar liposomes (prepared by reverse-phase evaporation) by Triton X-100, octyl glucoside, and sodium cholate. *Biochemistry.* 27:2668–2677.

Rigaud, J.-L., M. Paternostre, and A. Bluzat. 1988. Mechanisms of membrane protein insertion into liposomes during reconstitution procedures involving the use of detergents. 2. Incorporation of the light-driven proton pump bacteriorhodopsin. *Biochemistry.* 27:2677–2688.

Schubert, R., and K.-H. Schmidt. 1988. Structural changes in vesicle membranes and mixed micelles of various lipid compositions after binding of different bile salts. *Biochemistry.* 27:8787–8794.

Seliskar, C. J., and L. Brand. 1971. Electronic spectra of 2-aminonaphthalene-6-sulfonate and related molecules. I. General properties and excited-state reactions. *J. Am. Chem. Soc.* 93:5405–5420.

Seras, M., J. Galley, M. Vincent, M. Ollivon, and S. Lesieur. 1994. Micelle-vesicle transition of non-ionic surfactant-cholesterol assemblies induced by octyl glucoside: a time resolved fluorescence study of dehydroergosterol. *J. Coll. Interface Sci.* 167:159–171.

Seras, M., R. M. Handjani-Villa, M. Ollivon, and S. Lesieur. 1992. Kinetic aspects of the solubilization of non-ionic monoalkyl amphiphile-cholesterol vesicles by octylglucoside. *Chem. Phys. Lipids.* 63:1–14.

Seras, M., M. Ollivon, K. Edwards, and S. Lesieur. 1993. Reconstitution of non-ionic monoalkyl amphiphile-cholesterol vesicles by dilution of lipids-octylglucoside mixed micelles. *Chem. Phys. Lipids.* 66:93–109.

Szoka, F., and D. Papahadjopoulos. 1978. Procedure for preparation of liposomes with large internal aqueous space and high capture by reverse-phase evaporation. *Proc. Natl. Acad. Sci. USA.* 75:4191–4198.

Tanford, C. 1980. Mixed micelles. *In* The Hydrophobic Effect: Formation of Micelles and Biological Membranes, 2nd ed. Wiley, New-York.

Ueno, M. 1989. Partition behavior of a nonionic detergent, octyl glucoside, between membrane and water phases, and its effect on membrane permeability. *Biochemistry.* 28:5631–5634.

Urbaneja, M. A., A. Alonso, J. M. Gonzales-Manas, F. Goni, M. A. Partearroyo, M. Tribout, and S. Paredes. 1990. Detergent solubilization of phospholipid vesicles. Effect of electric charge. *Biochem. J.* 270:305–308.

Vinson, P. K., Y. Talmon, and A. Walter. 1989. Vesicle-micelle transition of phosphatidylcholine and octyl glucoside elucidated by cryo-transmission electron microscopy. *Biophys. J.* 56:669–681.

Walter, A. 1990. Membrane solubilization with and reconstitution from surfactant solutions: a comparison of phosphatidylserine and phosphatidylcholine interactions with octyl glucoside. *Mol. Cell. Biochem.* 99:117–123.

Walter, A. 1992. Vesicle-micelle transitions of surfactant phospholipid systems. *In* Biomembrane Structure and Function—The State of the Art. B. P. Gaber and K. R. K. Easwaran, editors. Adenine Press, New York. 21–35.

Walter, A., O. Eidelman, M. Ollivon, and R. Blumenthal. 1991. Functional reconstitution of viral envelopes. *In* Membrane Fusion. J. Wilschut and D. Hoekstra, editors. Marcel Dekker, New York. 395–418.

Weber, G., and F. J. Farris. 1979. Synthesis and spectral properties of a hydrophobic fluorescent probe: 6-propionyl-2-(dimethylamino)naphthalene. *Biochemistry.* 18:3075–3078.